CHAPTER 6

Synergetic concrete shape and cable layout optimization of pre-stressed concrete (PSC) beams

6.1 Introduction

Pre-stressed concrete is a method of reinforcing concrete in which internal stresses are introduced to counteract the stresses that will be imposed when the concrete is in service. This results in a stronger and more durable concrete structure. The process of pre-stressing concrete involves the use of high-tensile steel cables, called pre-stressing strands, which are anchored to the concrete structure at one end and then stretched, or "tensioned," at the other end. Once the concrete has been poured and hardened around the strands, the strands are then released and the concrete is left in a state of compression. Another way of achieving pre-stressing is by post-tensioning. Post-tensioned concrete is a method of reinforcing concrete in which internal stresses are introduced after the concrete has been poured and hardened. This is in contrast to pre-tensioning, in which the internal stresses are introduced before the concrete is poured. The process of post-tensioning involves the use of high-tensile steel cables, called post-

tensioning tendons, which are placed inside the concrete structure after it has been poured and hardened. These tendons are anchored to the structure at both ends and then tensioned, or "stressed," using hydraulic jacks. Once the tendons have been tensioned, the anchors are locked in place, maintaining the pre-stress in the tendons and inducing compression in the concrete. This compression provides a counterforce to the external forces, such as weight and tension, that the structure will be subjected to during its lifetime. One of the main advantages of pre-stressed concrete is that it allows for the creation of thinner and more slender structures, while still maintaining a high level of strength and stability. This is because the pre-stressing forces counteract the tensile forces that would otherwise cause the concrete to crack and weaken over time. As a result, pre-stressed concrete is often used in the construction of bridges, buildings, and other structures that are subject to high loads and large spans. Another advantage of pre-stressed concrete is that it is less prone to cracking and deformation than conventional reinforced concrete. This is because the pre-stressing forces are applied uniformly throughout the structure, which helps to distribute the stresses more evenly. Also, in cables that are curved, an upward force is applied to the concrete, which can reduce or prevent downward bending. Additionally, the use of high-tensile steel cables allows for a more efficient transfer of forces, resulting in a stronger and more durable structure. One of the main disadvantages of pre-stressed concrete is that it is a relatively complex and labour-intensive process. The steel cables must be anchored and tensioned correctly in order for the pre-stressing forces to be effective, which requires careful planning and execution.

The modelling of pre-stressing cables in finite element analysis (FEA) is a complex and time-consuming task, as the interaction between the cable and concrete involves various phenomena. The cable exerts both longitudinal and transverse forces

on the concrete due to friction and curvature, which must be taken into account in the FEA model. Additionally, the cable's stiffness must also be considered in the analysis. Most researchers have idealized the cable as having a parabolic shape, which can result in inaccuracies in the FEA model. For continuous structures, the cable is often considered to consist of several parabolas, which can lead to discontinuities at the juncture of two parabolas. However, the actual cable profile is a smooth curve that passes through all spans, which must be taken into account for more accurate results. It is important to note that the cable's actual shape must be considered in the FEA model for more accurate results. Additionally, the interaction between the cable and concrete must also be taken into account, as the cable exerts both longitudinal and transverse forces on the concrete due to friction and curvature. Hence, the modelling of pre-stressing cables in FEA may be a complex and time-consuming task, but it is crucial for ensuring the safety and stability of the final structure.

In order to achieve more realistic modelling of the cable, this study utilizes a B-spline curve model to represent the cable's profile. This approach avoids the drawbacks of the traditional parabolic modelling method and enables the inclusion of factors such as the effects of the cable force on the concrete and friction loss. This model has been incorporated into finite element programs. To demonstrate the validity and suitability of the proposed approach, various known and unknown examples have been solved using the B-spline curve model. Furthermore, the study also takes into consideration the cable's force on concrete and friction loss, which are important factors that affect the behaviour of the cable and the structure it supports. This model has been integrated with shape optimization of concrete and synergetic layout optimization of the cables into finite element programs to achieve an optimized overall pre-stressed beam of different

spans. The study solves various examples to prove the effectiveness of this proposed approach.

As seen from the literature review in Chapter 2 much of the research conducted to optimize pre-stressed concrete structures (PSC) has focused on two main approaches. The first approach, determining the optimal concrete section for a given cable profile and force, involves evaluating different concrete section sizes and shapes to find the one that will provide the best performance under the given cable profile and force. The second approach, identifying the optimal cable profile and force for a given concrete dimension, involves evaluating different cable profiles and forces to find the ones that will provide the best performance for a given concrete dimension. While these two approaches have been widely studied, there is a lack of literature on the concurrent optimization of both the cable profile and concrete shape. The concurrent optimization of both cable profile and concrete shape is crucial to achieving the optimal PSC structure. This is a more complex and challenging task but it is necessary to fully optimize the structure and take into consideration the interaction between the cable profile and the concrete shape.

The present work focuses on filling this gap. In the present study, synergetic optimization of concrete shape and cable layout of PSC beam under different loading conditions is done. By synergetic optimization, it is meant that the shape of the concrete beam and its cable layout is changed at every iteration until a final shape and cable layout are reached, which satisfies the convergence criteria. The concrete is modelled in a similar way as done before using nine-noded lagrangian elements, while the pre-stressing cable is modelled as a curvilinear three-noded bar element (Buragohain et al.,1993 &1997) laid following a third-order B-spline profile. The entire approach of synergetic optimization is again coded in FORTRAN and the software is labelled as

"Simultaneous Shape and Cable Optimization" (SSCO). Beams with different numbers of spans and different loading are optimized using SSCO as examples to show the efficacy of the proposed approach.

6.2 B-Spline curve

A B-spline curve is a type of mathematical function that is used to represent a smooth curve in computer graphics and other fields. It is a powerful tool that allows engineers and designers to create detailed models of complex shapes and structures. B-Spline curves are defined by a set of control points, which are used to control the shape and position of the curve. These control points are connected by a series of smooth spline segments, which are used to create the final curve. The resulting curve is a smooth, continuous function that can be used to represent a wide range of shapes and structures. One of the key advantages of B-Spline curves is their flexibility. Because the curve is defined by a set of control points, it is easy to adjust the shape and position of the curve by simply moving or modifying these control points. This makes it easy to create detailed models of complex shapes and structures, and to make changes to these models as needed. Another advantage of B-spline curves is that they can be used to represent a wide range of shapes and structures. This includes simple curves, such as circles and ellipses, as well as more complex shapes, such as the outlines of characters or other objects. B-spline curves can also be used to create models, which can be used in computer-aided design (CAD) and other applications. B-spline curves are used in structural engineering, architecture, automotive design, and aerospace engineering. This is because they are a powerful tool that can be used to create detailed models of complex shapes and structures, and to make changes to these models as needed. The ability to adjust the shape and position of the curve by simply moving or modifying

control points, makes it an ideal tool for optimization and representation of structures, such as pre-stressed cable where the cable profile is modelled as a B-spline curve to avoid the drawbacks of parabolic modelling and enable the inclusion of various factors such as the effects of the cable force on the concrete and friction loss.

If a single polynomial or cubic curve is used to simulate cable in continuous constructions such that it passes through the specified locations, a highly zigzag form is created. Because of this, the experts have regarded each span of wire as a distinct parabolic curve. The pre-stressing cable is modelled as a parabola since doing so eliminates the challenges of measuring the transverse force on concrete caused by cable tension. For each parabola, a constant load that is equally distributed is obtained using the load balancing principle.

Here in the present study to represent the profile of cable in a more realistic manner use of the B-spline curve is employed. This B-spline curve is a typical curve presented in the CAD methodology (Qing and Ding 1989, Rogers and Adams 1990). It simulates a smoothed curve between the specified ordinates. Researchers such as Braibant and Fleury (1984), Pourazady et al. (1996), Ghoddosian (1998), Akhtar et al. (2008), Yoely et al. (2018), Zelickman and Amir (2021) and others have employed this curve in shape optimization problems.

Schoenberg (1946) was the one who initially put out the B-spline hypothesis. Cox (1972) and de Boor (1978) separately established a recursive definition suitable for numerical computing. The B-spline basis was then used to define curves by Gorden and Resenfield (1974). Following is a basic explanation of the B-spline curve, and Rogers and Adams (1989) provide a more thorough explanation.

Assuming the position vector as P(t) along the B-spline curve. The P(t) can then be expressed by Equation 6.1

$$P(t) = \sum P_i . N_{i,k}(t) \qquad 0 < t < n - k + 2,\ 2 \leq k < n \tag{6.1}$$

Where,

$$N_{i,1} = \begin{cases} 1 & if\ x_i \leq t \leq x_{i+1} \\ 0 & otherwise \end{cases}$$

And,

$$N_{i,k}(t) = \frac{(t - x_i)N_{i,k-1}(t)}{(x_{i+k-1} - x_i)} + \frac{(x_{i+k} - t)N_{i+1,k-1}(t)}{(x_{i+k} - x_{i+1})}$$

For the aforementioned equations, *k* stands for the order of B-spline, $P_i$stand for *n+1* defining polygon vertices and $N_{i,k}(t)$ stands for the weighting function. In order to account for the inherent increased flexibility of B-spline curves, an extra knot vector called *x* is utilised. A knot vector can be simply put as a series of real integers x_i such that $x_i \leq x_i + 1\ \forall\ x_i$. They serve as an indicator of the parameter 't' which is implemented for the creation of the B-spline curve. Geometrical regularity is naturally taken into consideration whenever a B-spline curve is employed.

6.2.1 Properties of the B-spline Curve

The B-spline curve has the following key characteristics.

i. The curve shows the characteristics of variation diminishing. As a result, the curve doesn't quite oscillate over any straight line more frequently than its constituting polygon.

ii. In comparison to a Bezier curve, a B-spline curve polynomial's degree is independent of the number of control points.

iii. Typically, the curve mimics the constituting polygon's shape.

iv. The curve is positioned between the constituting polygon's convex hull. Without altering the number of constituting polygon vertices, the order of the resultant curve can be modified.

v. Smoothness: B-spline curves are smooth, continuous functions that can be used to represent a wide range of shapes and structures. This smoothness is achieved through the use of spline segments that connect the control points.

vi. Flexibility: B-spline curves are defined by a set of control points, which can be easily adjusted to change the shape and position of the curve. This makes it easy to create detailed models of complex shapes and structures and to make changes to these models as needed.

vii. Local control: Because B-spline curves are defined by a set of control points, changes to the curve can be made locally, by adjusting only the control points that are closest to the area of the curve that needs to be modified. This allows for fine-tuning the curve without affecting the rest of the shape.

viii. Interpolation: B-spline curves can be used to interpolate a set of data points, creating a smooth curve that passes through all of the data points. This is useful for creating detailed models of complex shapes and structures.

ix. Approximation: B-spline curves can also be used to approximate a set of data points, creating a smooth curve that is close to the data points but does not pass through all of them. This is useful for creating detailed models of complex shapes and structures.

x. Dimensionality: B-spline curves can be used in both two-dimensional and three-dimensional applications, making them versatile and adaptable to different structures.

xi. Capability of modelling non-uniformly distributed data: B-spline curve can be used to model non-uniformly distributed data, where the data is not evenly spaced. This is useful for creating detailed models of complex shapes and structures where the data points are not evenly spaced.

xii. The capability of modelling any shape: The B-spline curve can model any shape, unlike some other curve-fitting methods that have limitations in modelling certain types of shapes.

xiii. The capability of modelling both open and closed shapes: B-spline curves can be used to model both open and closed shapes, making them versatile and adaptable to different structures.

The B-spline basis transforms to a Bezier curve once the number of constituting polygon vertices is equal to the order of the B-spline basis.

6.3 Methodology

The technique proposed here optimizes the concrete shape and cable layout of PSC beams in a mutually cooperative way focusing on the removal of tensile stress. The strategy exercised for the same is to move the design node/s modifying the shape of boundary followed by modification of cable layout in accordance to the modified shape of concrete targeting removal of tensile stress. This entire procedure is executed at each iteration until the criteria of convergence are met, and a final optimized concrete shape and cable layout for the given load and pre-stressing force is obtained.

In order to analyse the pre-stressed concrete components, the following assumptions have been made:

i. The cable segment has B-spline geometry, which is determined by two points at either end and a third point in the middle of the segment's length.

ii. There exists a perfect bond between the cable and concrete.

iii. Consideration of frictional loss in the cable is factored in.

iv. The cable duct's effect on the concrete's deterioration is taken into consideration.

6.3.1 Finite element modelling of cable

The finite element analysis of pre-stressed concrete structures requires modelling the pre-stressing cable, which is a laborious process. Based on the cable profile, the cable pressure on concrete is determined. Therefore, accurate cable modelling is a crucial aspect of the study. There is a perfect bond between the cable and the concrete, which is regarded to be embedded in it. The dead and live loads imposed on the beam are counterbalanced by the cable using its curvature. A highly smooth contour is produced by the cable profile modelled using B-splines. In the current study, the cable is taken as a curvilinear three-noded bar element embedded in the concrete element, as depicted in Figure 6.1. The shape function and global co-ordinates of the curved bar can be expressed by Equation 6.2 and Equation 6.3, respectively.

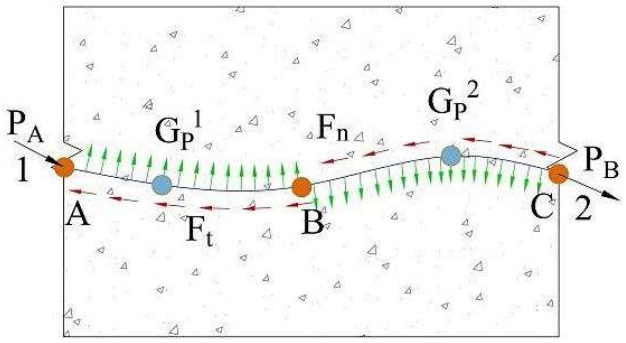

Figure 6.1: Three-noded curved bar element embedded in concrete and the transfer of force from cable to concrete

$$S_c^1 = \frac{\zeta(\zeta-1)}{2}, S_c^2 = (\zeta+1)(1-\zeta), S_c^3 = \frac{\zeta(\zeta+1)}{2} \quad (6.2)$$

$$X = \begin{Bmatrix} x \\ y \end{Bmatrix} = \sum_{i=1}^{3} \begin{Bmatrix} x \\ y \end{Bmatrix} S_c^i = \sum_{i=1}^{3} X_i \, S_c^i \tag{6.3}$$

The tangential and normal vectors along the ζ axis for the cable can be expressed using Equation 6.4.

$$\left.\begin{aligned} \bar{T} &= \sum_{i=1}^{3} X_i \frac{dS_c^i}{d\zeta} \\ \bar{N} &= \frac{1}{|\bar{T}|^2}\left(\frac{d^2X}{d\zeta^2} - \frac{a}{|\bar{T}|^2}\frac{dX}{d\zeta}\right) \end{aligned}\right\} \tag{6.4}$$

Where, $a = \frac{dX}{d\zeta}.\frac{d^2X}{d\zeta^2}$

The radius of curvature of a cable at any point can be expressed as the reciprocal of curvature (K) at that point on the cable curve and can be expressed using Equation 6.5:

$$K = \frac{\left|\frac{dX}{d\zeta}.\frac{d^2X}{d\zeta^2}\right|}{\left(\left|\frac{dX}{d\zeta}\right|^2\right)^{\frac{3}{2}}}, \text{ and } R = \frac{1}{K} \tag{6.5}$$

6.3.2 Load Transfer

The cable forces transferred to the concrete are tangential and normal in nature at the points of contact, as depicted in Figure 6.1. Taking P_n as tension in the cable and $\bar{t}$ and $\bar{n}$ as unit tangent and normal vectors respectively, the tangential and normal force can be expressed using Equation 6.6 and the resultant force can be expressed using Equation 6.7.

$$\left.\begin{aligned} F_t &= \frac{dP_n}{dX} = \frac{1}{|\bar{T}|}.\frac{dP_n}{d\zeta} \\ F_n &= \frac{P_n}{R} \end{aligned}\right\} \tag{6.6}$$

$$\bar{F} = F_t \bar{t} + F_n \bar{n} \tag{6.7}$$

The loads are then transferred to the finite element nodes, for which the concept of virtual work is adopted. The anchored ends of the cable produce reaction force which acts as concentrated loads on concrete end elements. These forces are transmitted in the ratio of their shape function to their nodes. The equivalent nodal force vector and anchored force vector for a concrete element can be expressed using Equations 6.8 and 6.9 respectively.

$$\{F_L\} = \int_{-1}^{1} [S]^T \{\bar{F}\} |\bar{T}| \, d\zeta \tag{6.8}$$

$$\{F_A\} = [S]^T . \{P_{end}\} \tag{6.9}$$

Where, P_{end} denotes the tension in cables at end nodes, and S denotes the shape function vector for nine-noded elements. In order to calculate Equation 6.8, the local co-ordinates of anchorage points are needed from their available global co-ordinates. This inverse non-linear problem is solved using the Newton-Raphson method. The computation follows an iterative procedure which terminates when the difference between two consecutive values of local co-ordinates falls within the tolerance limit. Assuming global co-ordinates as (x, y) and local co-ordinates as (ξ, η). The local co-ordinates can be obtained using Equation 6.10:

$$\begin{Bmatrix} \xi \\ \eta \end{Bmatrix}_{i+1} = \begin{Bmatrix} \xi \\ \eta \end{Bmatrix}_{i} + \begin{bmatrix} \frac{\partial x}{\partial \xi} & \frac{\partial x}{\partial \eta} \\ \frac{\partial y}{\partial \xi} & \frac{\partial y}{\partial \eta} \end{bmatrix}^{-1} \begin{Bmatrix} x_{i+1} - x_i \\ y_{i+1} - y_i \end{Bmatrix} \tag{6.10}$$

Where the (x_i, y_i) and (x_{i+1}, y_{i+1}) are the known and computed values of global co-ordinates respectively, and the inverse matrix is the Jacobian matrix. The initial value of (ξ, η) is (0, 0) with a tolerance of 0.01. The total load vector because of cable concrete interaction can be expressed using Equation 6.11. This total load combined with dead load and imposed live load is applied to the finite element model to calculate the overall pre-stressing effects.

$$\{F_{final}\} = \{F_L\} + \{F_A\} \tag{6.11}$$

6.3.3 Friction loss

For the consideration of loss due to friction, the curvilinear bar element is assumed to have two Gauss points G_P^1 & G_P^2 and the tension variation for the same is expressed using iso-parametric interpolation as given in Equation 6.12.

$$P_n = \sum_{i=1}^{3} P_i S_c^i \tag{6.12}$$

Assuming the radii of curvature between A-B and B-C as R_1 & R_2, P_A as tension at the jacking end for the first element, μ as the coefficient of friction, and ω as the wobble coefficient, the cable tension at B & C after friction loss can be expressed using Equation 6.13

$$\left.\begin{aligned} P_B &= P_A e^{(-\mu\alpha_1 - \omega L_{A-B})} \\ P_C &= P_B e^{(-\mu\alpha_2 - \omega L_{B-C})} \end{aligned}\right\} \tag{6.13}$$

Where, $\alpha_1 = L_{A-B}/R_1$, $(L_{A-B} = \sqrt{(X_A - X_B)^2 + (Y_A - Y_B)^2})$ and

$\alpha_2 = L_{B-C}/R_2$, $(L_{B-C} = \sqrt{(X_B - X_C)^2 + (Y_B - Y_C)^2})$

For subsequent elements P_A will become P_C of their previous elements.

6.4 Shape optimization of concrete

The concrete for shape optimization is characterized as a discrete continuum following the finite element-based methodology as explained in Chapter 1 of this thesis. However, a brief description of the methodology and changed parameters is being discussed here. The beam is segmented into appropriate parts as design elements and then further discretized into nine-noded lagrangian elements. Automatic mesh is created and refined at each iteration for the changed shape using Auto Mesh Creator and Refiner (AMCR). The boundary of the design elements is determined using a two-dimensional iso-parametric interpolation function. The key-node/s prevailing at these boundaries are taken up for the process of optimization and hence termed as design nodes. The key-nodes move to change the shape of the boundary. Assuming i^{th} node as the design node and j^{th} node as the direction node, the extent of movement of i^{th} node having co-ordinate (X_i, Y_i) towards direction node 'j' having co-ordinate (X_j, Y_j) is evaluated using move value (MV) which is dependent on move factor (MF) and the shortest length (M_{min}) traversed between the direction node and its key-node. The MV can be expressed using Equation 6.14. The present study's nodal movement has been limited to one-fourth of the M_{min}.

$$\text{MV}(i) = 0.25 \cdot M_{min} \cdot \text{MF} \tag{6.14}$$

Where, M.F. = [1 - $\psi(\sigma_i)$] , $M_{min} = \min_{i=1}^{N_d} (M_i)$, $M_i = \sqrt{(X_i - X_j)^2 + (Y_i - Y_j)^2}$

$\psi(\sigma_i)$ is the triangular membership function value for that iteration, and N_d is the total number of key-node.

The co-ordinates of the design node '*i*' change at each iteration, and the freshly acquired co-ordinates X_i' and Y_i' is represented using Equation 6.15.

$$\left.\begin{aligned} X_i' &= X_i + (X_j - X_i) \cdot \frac{MV(i)}{M_i} \\ Y_i' &= Y_i + (Y_j - Y_i) \cdot \frac{MV(i)}{M_i} \end{aligned}\right\} \quad (6.15)$$

The optimizer takes the new co-ordinates and sends them to the mesh generator, which generates a new mesh based on the newly obtained co-ordinates.

6.5 The layout design algorithm

The cable layout is modified at every iteration until either of the two convergence criteria is reached. The two criteria are:

i. The tensile stress is completely removed.

ii. The minimum concrete cover of 40 mm (for the present study) is reached.

The second convergence criterion ensures that the cable always remains embedded in concrete with minimum cover (can be defined by the user) maintained. Hence, the aim is to reduce the tensile stress in the concrete up to the acceptable limit, which is below 0.5 N/mm^2 in the present study. The cable is initially laid straight between the anchorage ends and then modified at every iteration as the analysis progresses, following a third-order B-spline curve profile. The convex hull property of the B-spline ensures that the curve is contained within the convex hull of its control points, while the movement of ordinates of the control points determines the overall shape. A schematic representation of a 3-span beam can be seen in Figure 6.2, which shows 7 control points with 3 control points per span (or per design element as 1 span is rendered as 1 design element here). Out of these 7 control points, the 5 control points are allowed to move during optimization in order to counter the tensile stress. The ordinates move downwards or upwards in order to remove tensile stress from the

concrete. This can be categorized into the following three cases, as presented in Table 6.1.

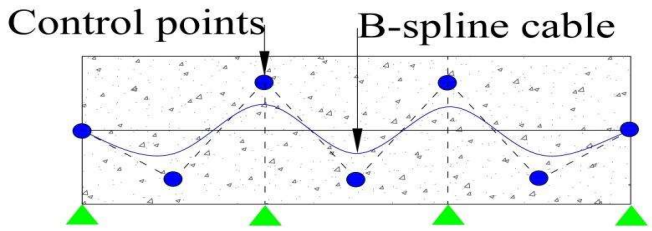

Figure 6.2: B-spline model of cable geometry for 3-span beam.

Table 6.1: Calculation of B-spline ordinates

Top fibre	**Bottom fibre**	**Calculation of new Y-co-ordinate of B-spline ordinates**
Tension	Compression	$y_{i+1} = (1+Q)y_i$ where, $Q = \frac{\sigma_{it}}{\sigma_{it}+\lvert\sigma_{ib}\rvert}$
Compression	Tension	$y_{i+1} = (1-Q)y_i$ where, $Q = \frac{\sigma_{ib}}{\sigma_{ib}+\lvert\sigma_{it}\rvert}$
Compression	Compression	No need to change the cable profile.

6.6 Problem formulation

The present study takes into account the synergetic optimization of concrete shape and pre-stressing cable profile of pre-stressed beams to counter the tensile stresses created due to the imposed load. The concrete as presented in section 6.4, is modelled as a discretized continuum using nine-noded lagrangian elements, while the cable is modelled as a curvilinear three-noded bar element tracing a B-spline profile. The PSC beam is analysed using finite element analysis (FEA). Since the process focuses on minimizing the tensile stress while reducing the concrete weight of the PSC beam, the objective functions to be minimized are stress (σ_k) at all the nodes and the concrete weight ($W_{concrete}$) of the PSC beam. The overall weight of a PSC beam includes the weight of concrete and the tendons, but in the present study, the weight of the tendons is

disregarded. To fulfil these objectives, the design variables selected are B-spline ordinates of the cable and design-node/s of concrete. The overall optimization problem is constraint using four criteria which also serve as the criteria for convergence. The four criteria are (i) stress limits (to be defined by the user), (ii) minimum concrete cover (MCC) (to be defined by the user), (iii) maximum deflection (δ) at any point, and (iv) concrete weight reduction. Upon the fulfilment of these four requirements, it is determined that convergence has been successfully attained, and the optimization procedure is terminated. The complete optimization problem for the present study can be formulated mathematically using Equation 6.16.

$$\text{Minimize} \quad \sigma_k \ (\forall\ \mathrm{k} = 1 \text{ to n}) \text{ and } W_{concrete} = \sum_{e=1}^{m} \gamma_e . A_e . B_e \tag{6.16}$$

Subjected to

- -40 N/mm^2 $\leq \sigma_k \leq$ +0.5 N/mm^2 ('-' denotes compression and '+' denotes tension) (Limits can be changed as per user requirements)
- MCC $\geq$ 40 mm (Can be changed as per user requirements)
- Deflection (δ) $\leq$ Minimum ($Span/250$, 20 mm)
- $W_{concrete\ final} < W_{concrete\ initial}$

Where n is the total number of nodes, m is the total number of elements, γ_e denotes the density of the concrete, A_e denotes the area of the element and B_e stands for the breadth of the element.

6.7 Software SSCO

The author has created a FORTRAN code coined SSCO to analyse and optimize pre-stressed concrete structures using the approach mentioned above. The code uses finite element analysis with a 9-node plane stress element for concrete and a 3-node curved bar element for the cable. The software consists of 12 main subroutines. The programs

have been successfully executed on a Ryzen 5 processor using the Microsoft Fortran PowerStation 4. Some of the subroutines are shared with the GSO software discussed in Chapter 3. A brief explanation of these subroutines is provided below.

a) **Subroutine INPUT:** This subroutine is similar to the INPUT subroutine of the GSO software but with additional input parameters for cable modelling. These include the number and direction of cables, the number of B-spline points and their ordinates, and the tension in the cables.

b) **Subroutine LOADPS:** This is a subroutine that has already been mentioned in Chapter 1.

c) **Subroutine GEOM:** This subroutine calculates the three co-ordinates of the cable in an element, allowing it to be modelled as a 3-node bar element.

d) **Subroutine PREST:** This subroutine computes the friction loss, curvatures in the cable, and normal and tangential cable forces on the concrete, and translates them into equivalent nodal forces.

e) **Subroutine STIFFP:** This subroutine is identical to the one previously discussed in Chapter 1.

f) **Subroutine ASSEMBL:**This subroutine is identical to the one previously discussed in Chapter 1.

g) **Subroutine GREDUC:** This subroutine is identical to the one previously discussed in Chapter 1.

h) **Subroutine BACKSUB:** This subroutine is identical to the one previously discussed in Chapter 1.

i) **Subroutine DISPLAC:** This subroutine is identical to the one previously discussed in Chapter 1.

j) **Subroutine GPSTRESS:** This subroutine is identical to the one previously discussed in Chapter 1.

k) **Subroutine SHAPENCABLE:** This subroutine optimizes the pre-stressed beam synergistically for the shape of concrete and cable layout.

l) **Subroutine OUTPUT:** This subroutine saves the stresses and displacements resulting from the finite element analysis for both friction and non-friction cases.

The whole process of SSCO can be summarized using the flowchart illustrated in Figure 6.3.

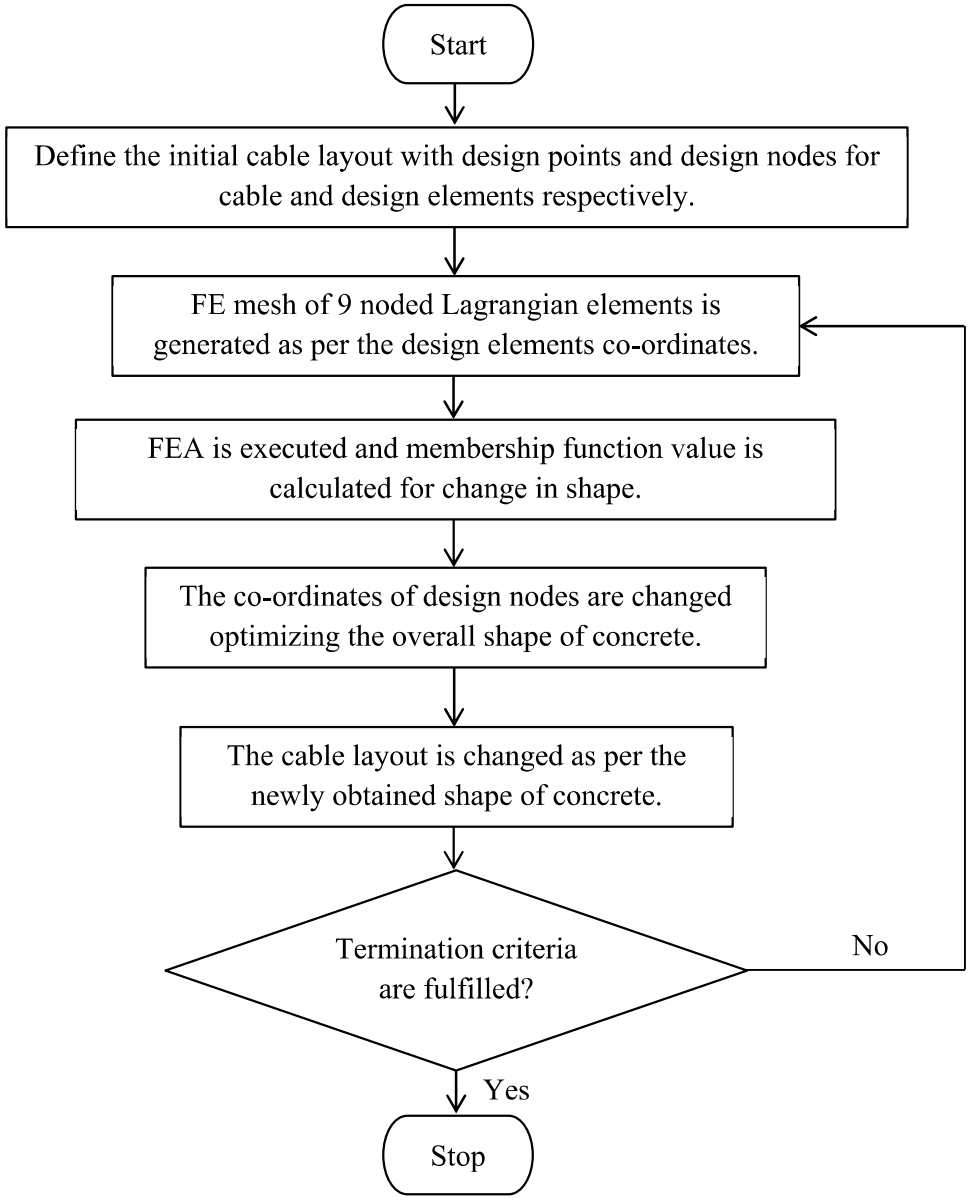

Figure 6.3: Flowchart for SSCO procedure

6.8 Validation and convergence study

For the convergence and validation study of the proposed methodology, the calculation of bending stress at the top (σ_{top}), bottom (σ_{bottom}) and central deflection (δ) of a simply

supported single-span PSC beam is done using SSCO under different mesh element size and the results are compared with the values obtained using the conventional formulae (CF) (Nawy 2009) for σ_{top}, σ_{bottom} and δ of a simply supported single span PSC beam. The beam have dimensions (3000x150x300)mm and is loaded uniformly with an 18kN/m load throughout the span. The cable is laid straight at a uniform eccentricity of 75mm. The material properties of concrete taken is ($E = 3.8x10^4$ N/mm^2, $\rho = 2.5\ x10^{-5}$ N/mm^3 and $\nu = 0.15$) and of cable taken is ($E = 2.1x10^5$ N/mm^2, $\rho = 7.85\ x10^{-5}$ N/mm^3 and $\nu = 0.3$). The PSC beam is rendered with a single design element with further division into nine noded lagrangian elements having element size varied in Y-axis/ X-axis as 300/500 to 150/125. The outcome of the study is presented graphically in Figure 6.4. It can be observed that the convergence is achieved at an element size of 300/250. The use of nine noded elements in the present study has allowed us to attain substantially accurate values without necessitating to have fine mesh. Consequently, the element size of 300 on the Y-axis to 250 on the X-axis is used successively hereafter for further analysis in SSCO.

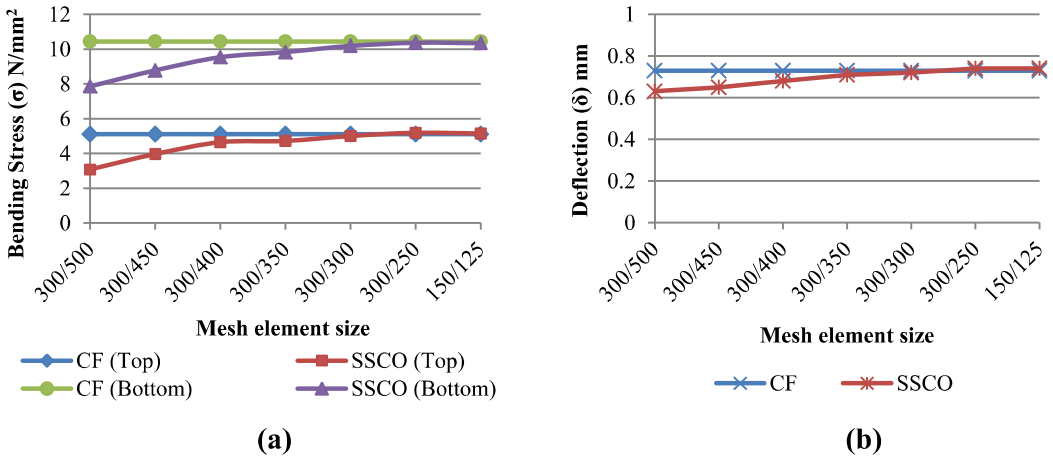

Figure 6.4: Convergence and validation study (a) based on bending stress 'σ' (b) based on deflection (δ)

6.9 Numerical illustrations

Three types of PSC beams P_{B1}, P_{B2}, and P_{B3} having one, three and five spans respectively are modelled and optimized for both concrete shape and cable layout using SSCO. All the PSC beams are initially rectangular with prismatic cross-sections and cable laid straight at the neutral axis. The material properties for the concrete is taken as E = 3.5x104 N/mm^2, ρ = 2.5 x10-5 N/mm^3 and ν = 0.15 and for the cable is taken as E = 2.1x105 N/mm^2, ρ = 7.85 x10-5 N/mm^3 and ν = 0.3 The PSC beams are then optimized under the imposed loading and pre-stressing force using SSCO and compared with the initial non-optimized state on the basis of three parameters, viz. (a) the bending stress at the top (σ_{top}) and bottom (σ_{bottom}) at each marked section between the supports in each span, (b) the deflection (δ) (downward +ve and upward –ve) at each marked section between the supports in each span, and (c) the percentage weight reduction. All of these data for beams P_{B1}, P_{B2}, and P_{B3} are given in Tables 6.2, 6.3, and 6.4 respectively. The final optimized concrete shape and cable layout of P_{B1}, P_{B2}, and P_{B3} are presented in Figures 6.6, 6.8, and 6.10 respectively. The stress distribution for initial non-optimized and final optimized beams P_{B1}, P_{B2}, and P_{B3} and its variation in cable layout due to the ignorance and consideration of frictional loss is also exhibited.

6.9.1 Single-span PSC beam (P_{B1})

P_{B1} is a single span simply supported PSC beam having length, breadth and height of 3000mm, 250mm and 300mm respectively. The beam is rendered as a single design element, with further sub-division in nine noded lagrangian finite elements having element size ratio of length to height as 0.8:1 approx. Two cases of loading have been considered here (i) a point load (PL) of 125kN at the mid of the span and (ii) an uniformly distributed load (UDL) of 75N/mm acting vertically down throughout the

span. A pre-stressing force of 500kN is applied at the jacking end, with loss due to friction ignored. The beam is optimized at the middle section (Section 1-1) only keeping the support ends constant for shear stress consideration. The problem is then executed using SSCO, and the three parameters (a) σ_{top} and σ_{bottom}, (b) δ, and (c) percentage weight reduction achieved along with the total number of iterations and total runtime is presented in Table 6.2. The stress distribution plot of the non-optimized beam P_{B1} under PL and UDL loading is presented in Figure 6.5. The optimized concrete shape and cable layout along with the stress plot of P_{B1} is depicted in Figure 6.6. All dimensions are in 'mm' unless otherwise stated.

Table 6.2: Single-span PSC beam. (P_{B1})

Loading	Stage	Section	Bending stress		Deflection δ (mm)	Iteration (Nos.)	Runtime (sec.)	Weight Reduction (%)
			σ_{top}	σ_{bottom}				
125 kN (PL)	Initial	1-1	-32.72	17.37	3.67	3	0.14	16.76
	Optimized		-40.81	-12.79	1.56			
75 N/mm (UDL)	Initial	1-1	-29.22	15.88	4.13	3	0.17	16.52
	Optimized		-36.86	-16.71	2.32			

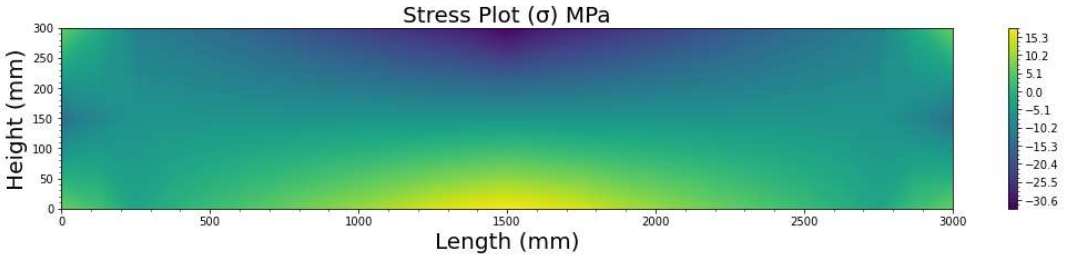

(a)

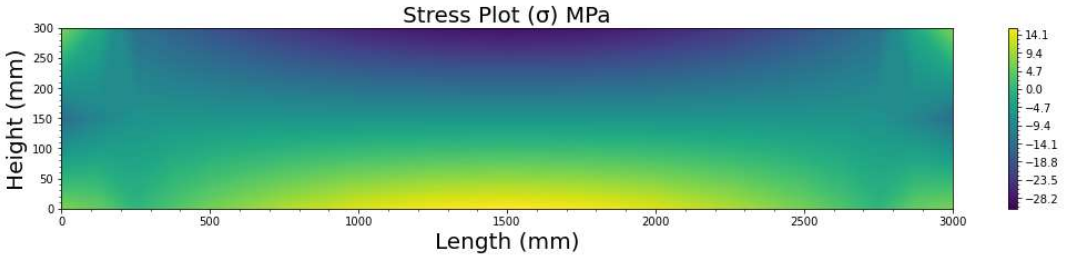

(b)

Figure 6.5: Stress distribution plot of non-optimized beam P_{B1} under (a) PL, and (b) UDL

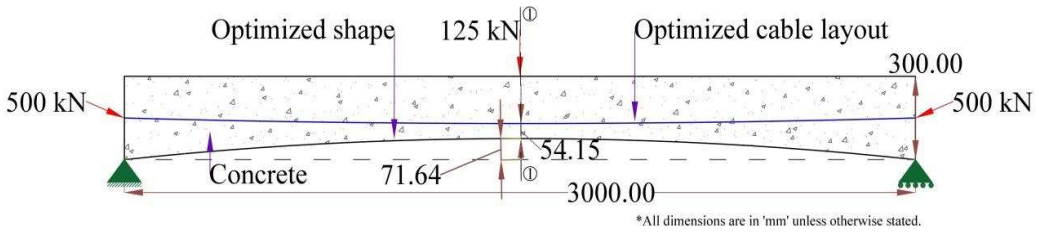

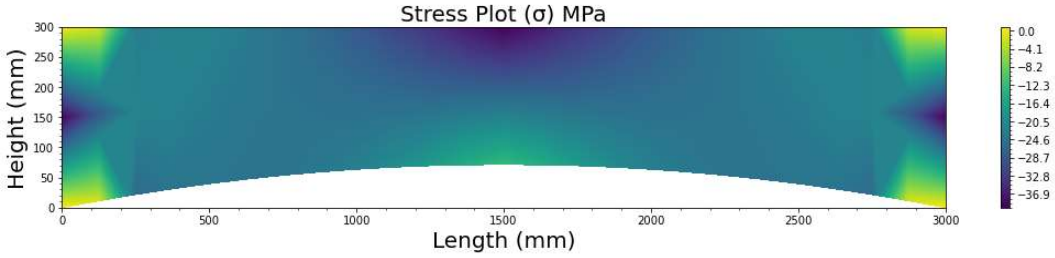

(a)

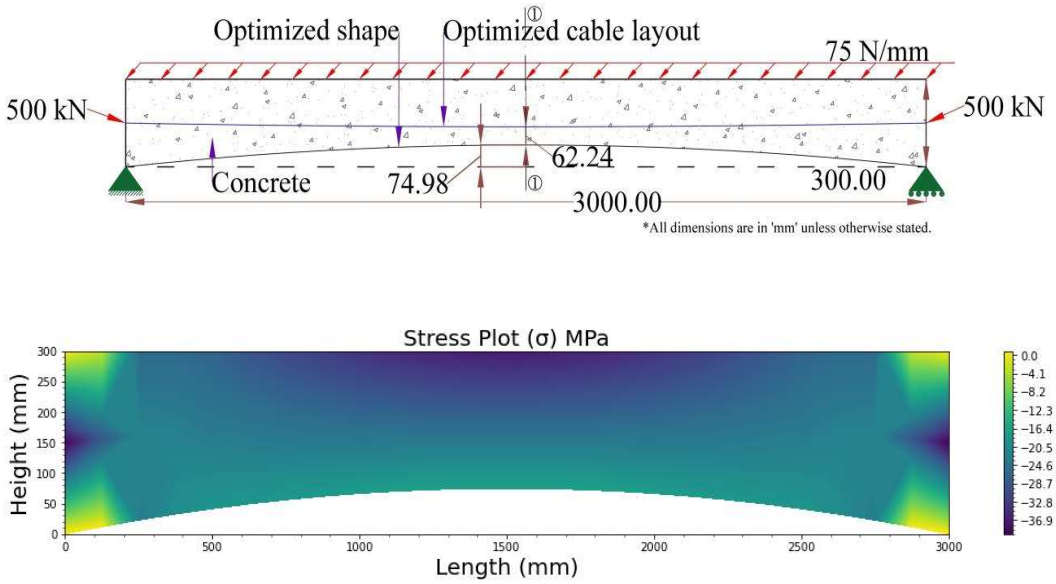

(b)

Figure 6.6: Optimized concrete shape, cable layout and Stress distribution plot of P_{B1} for (a) PL (b) UDL

6.9.2 Three-span PSC beam (P_{B2})

P_{B2} is a three-span simply supported PSC beam having length, breadth and height as 9000mm, 500mm and 600mm respectively. The beam is divided into three design elements, with further sub-division in nine noded lagrangian finite elements having element size ratio of length to height as 0.8:1 approx. Two different loading condition is considered (i) a point load (PL) of 500 kN at the mid of the span and (ii) an uniformly distributed load (UDL) of 111.11 N/mm acting vertically down throughout the length of the beam. The pre-stressing force of 900 kN and 400 kN under PL and UDL loading respectively is applied at the jacking end. Loss due to friction is being considered for P_{B2}. The beam is optimized at Sections 1-1, 2-2, and 3-3, as marked in Figure 6.8. The

intermediate supports are allowed to move as per the optimized concrete shape, whereas the end supports are kept fixed. The problem is then executed using SSCO, and the three parameters (a) σ_{top} and σ_{bottom}, (b) δ, and (c) percentage weight reduction achieved along with the total number of iterations and total runtime is presented in Table 6.3. The stress distribution plot of the non-optimized beam P_{B2} under PL and UDL loading is presented in Figure 6.7. The optimized concrete shape and cable layout along with the stress plot of P_{B2} is depicted in Figure 6.8. All dimensions are in 'mm' unless otherwise stated.

Table 6.3: Three-span PSC beam (P_{B2})

Loading	Stage	Section	Bending stress		Deflection δ (mm)	Iteration (Nos.)	Runtime (sec.)	Weight Reduction (%)
			σ_{top}	σ_{bottom}				
500 kN (PL)	Initial	1-1	-0.02	-5.73	-0.27	6	0.28	12.73
	Optimized	1-1	-1.66	-39.11	-1.83			
	Initial	2-2	-11.14	4.15	0.49			
	Optimized	2-2	-18.07	-9.73	0.78			
	Initial	3-3	0.09	-5.13	-0.25			
	Optimized	3-3	0.017	-34.86	-1.73			
111.11 N/mm (UDL)	Initial	1-1	-2.92	0.31	0.15	3	0.14	18.91
	Optimized	1-1	-4.53	-5.50	-0.06			
	Initial	2-2	-1.94	0.97	0.13			
	Optimized	2-2	-5.20	-0.03	0.35			
	Initial	3-3	-2.82	0.44	0.15			
	Optimized	3-3	-4.34	-4.71	-0.04			

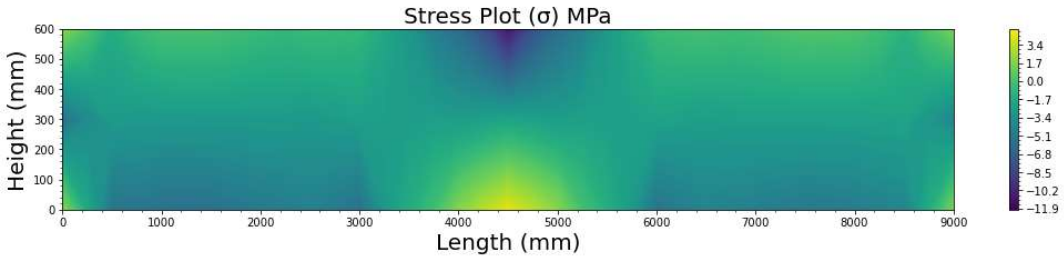

(a)

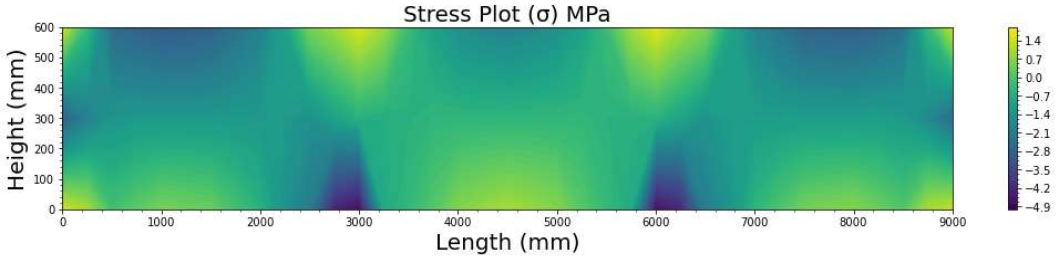

(b)

Figure 6.7: Stress distribution plot of non-optimized beam P_{B2} under (a) PL, and (b) UDL

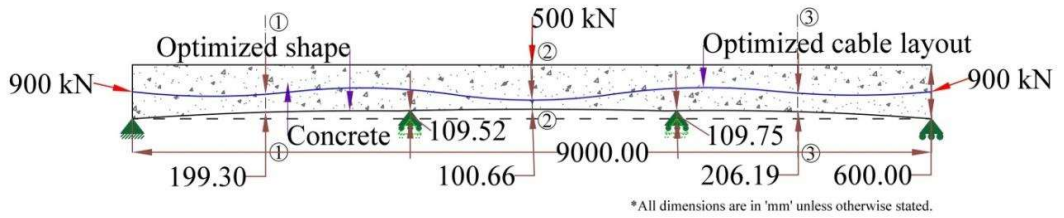

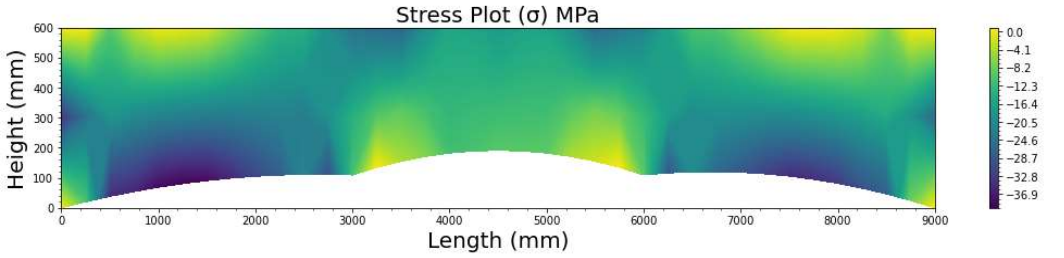

(a)

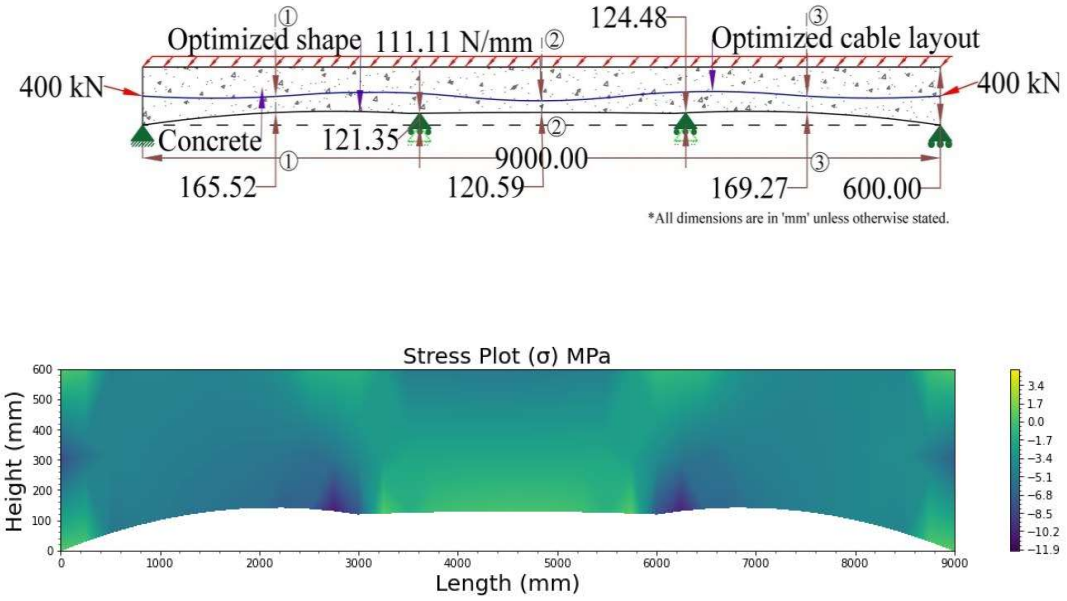

(b)

Figure 6.8: Optimized concrete shape, cable layout and Stress distribution plot of P_{B2} for (a) PL (b) UDL

6.9.3 Five-span PSC beam (P_{B3})

P_{B3} is a five-span simply supported PSC beam having length, breadth and height of 18000 mm, 600 mm and 1000 mm respectively. The beam is divided into five design elements, with further sub-division in nine noded lagrangian finite elements having element size ratio of length to height as 0.8:1 approx. Two different loading condition is considered (i) multiple point load (MPL) of 500 kN, 600kN, 700 kN, 600kN, and 500kN at section 1-1, 2-2, 3-3, 4-4, and 5-5 respectively, (ii) a uniformly increasing load (UIL) of 0 N/mm to 111.11 N/mm along the full length of the beam. A pre-stressing force of 900 kN at the jacking end is applied in both cases. Loss due to friction is being considered for $P_{B3,}$ and the variation in optimized concrete shape and cable layout due to ignorance and consideration of friction is presented in Figure 6.10. The beam is optimized at Sections 1-1, 2-2, 3-3, 4-4, and 5-5, as marked in Figure 6.10. The end and intermediate supports are kept fixed in their initial position. The problem is then executed using SSCO, and the three parameters (a) σ_{top} and σ_{bottom}, (b) δ, and (c) percentage weight reduction achieved along with the total number of iterations and total runtime is presented in Table 6.4. The stress distribution plot of the non-optimized beam P_{B3} under MPL and UIL loading is presented in Figure 6.9. The optimized concrete shape and cable layout along with the stress plot of P_{B3} is depicted in Figure 6.10. All dimensions are in 'mm' unless otherwise stated.

Table 6.4: Five-span PSC beam (P_{B3})

Loading		Stage	Section	Bending stress		Deflection δ (mm)	Iteration (Nos.)	Runtime (sec.)	Weight Reduction (%)
				σ_{top}	σ_{bottom}				
Frictional loss ignored	MPL	Initial	1-1	-4.24	0.36	0.13	4	0.58	20.94
		Optimized	1-1	-4.63	-13.78	-0.48			
		Initial	2-2	-3.58	1.69	0.16			
		Optimized	2-2	-6.71	-2.38	0.31			
		Initial	3-3	-3.76	2.05	0.17			
		Optimized	3-3	-2.25	-2.41	0.09			
		Initial	4-4	-3.58	1.69	0.16			
		Optimized	4-4	-6.70	-2.37	0.31			
		Initial	5-5	-4.24	0.36	0.13			
		Optimized	5-5	-4.64	-13.74	-0.47			
	UIL	Initial	1-1	-0.97	-2.01	-0.04	4	0.59	24.43
		Optimized	1-1	0.48	-20.21	-1.07			
		Initial	2-2	-1.05	0.13	0.07			
		Optimized	2-2	-4.09	-5.78	0.16			
		Initial	3-3	-0.76	0.45	0.08			
		Optimized	3-3	-0.48	-4.27	0.03			
		Initial	4-4	-1.51	0.84	0.13			
		Optimized	4-4	-4.78	-4.73	0.24			
		Initial	5-5	-3.74	0.81	0.23			
		Optimized	5-5	-2.32	-16.82	-0.68			
Frictional loss considered	MPL	Initial	1-1	-4.26	0.52	0.14	5	0.78	20.11
		Optimized	1-1	-5.29	-16.28	-0.62			
		Initial	2-2	-3.58	1.74	0.16			
		Optimized	2-2	-6.87	-3.26	0.25			
		Initial	3-3	-3.80	2.14	0.17			
		Optimized	3-3	-1.08	-2.53	0.01			
		Initial	4-4	-3.42	1.80	0.15			
		Optimized	4-4	-4.78	-1.21	0.18			
		Initial	5-5	-3.97	0.98	0.15			
		Optimized	5-5	-4.62	-8.43	-0.30			
	UIL	Initial	1-1	-0.99	-1.86	-0.04	4	0.67	23.77
		Optimized	1-1	0.50	-20.77	-1.14			
		Initial	2-2	-1.04	0.17	0.07			
		Optimized	2-2	-4.44	-4.97	0.19			
		Initial	3-3	-0.80	0.54	0.08			
		Optimized	3-3	-0.58	-3.09	0.05			
		Initial	4-4	-1.36	0.95	0.12			
		Optimized	4-4	-2.68	-2.83	0.16			
		Initial	5-5	-3.46	1.43	0.24			
		Optimized	5-5	-3.50	-9.21	-0.23			

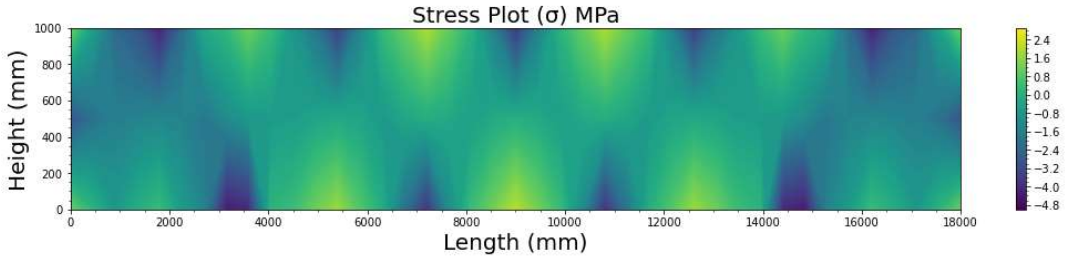

(a)

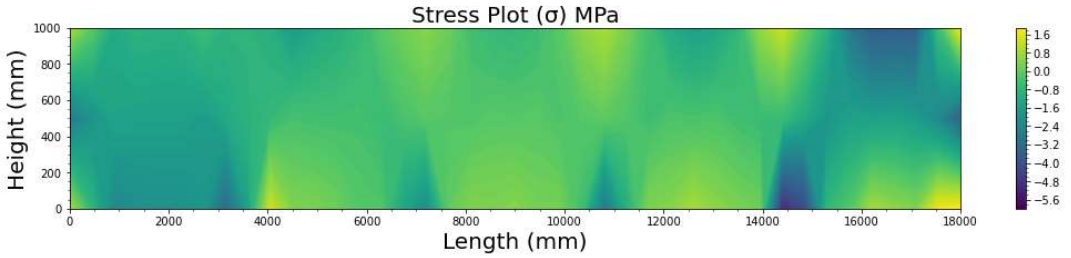

(b)

Figure 6.9: Stress distribution plot of non-optimized beam P_{B3} under (a) MPL, and (b) UIL

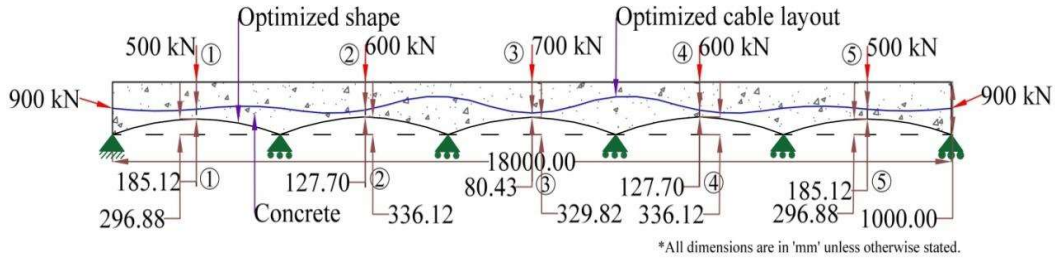

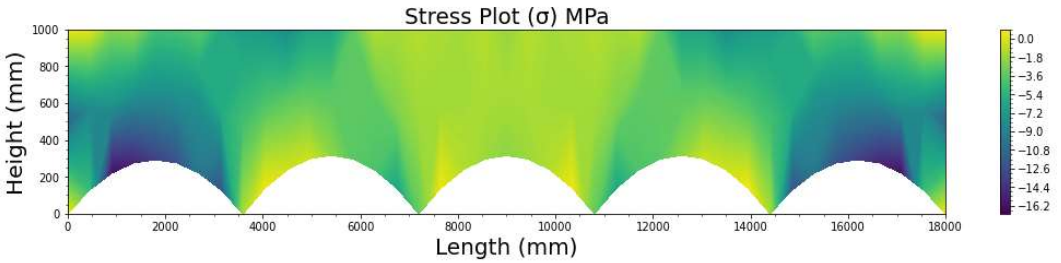

(a)

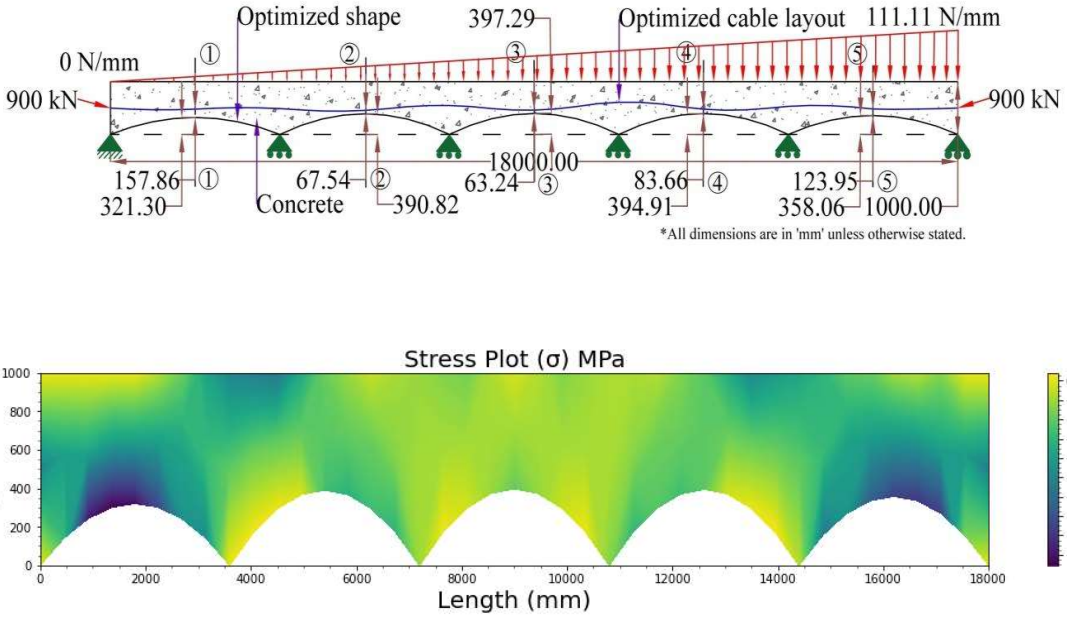
Optimized shape
397.29
Optimized cable layout
111.11 N/mm
0 N/mm
900 kN
900 kN
157.86
321.30
67.54
Concrete
390.82
18000.00
63.24
83.66
394.91
123.95
358.06
1000.00
*All dimensions are in 'mm' unless otherwise stated.
Stress Plot (σ) MPa
Height (mm)
Length (mm)

(b)

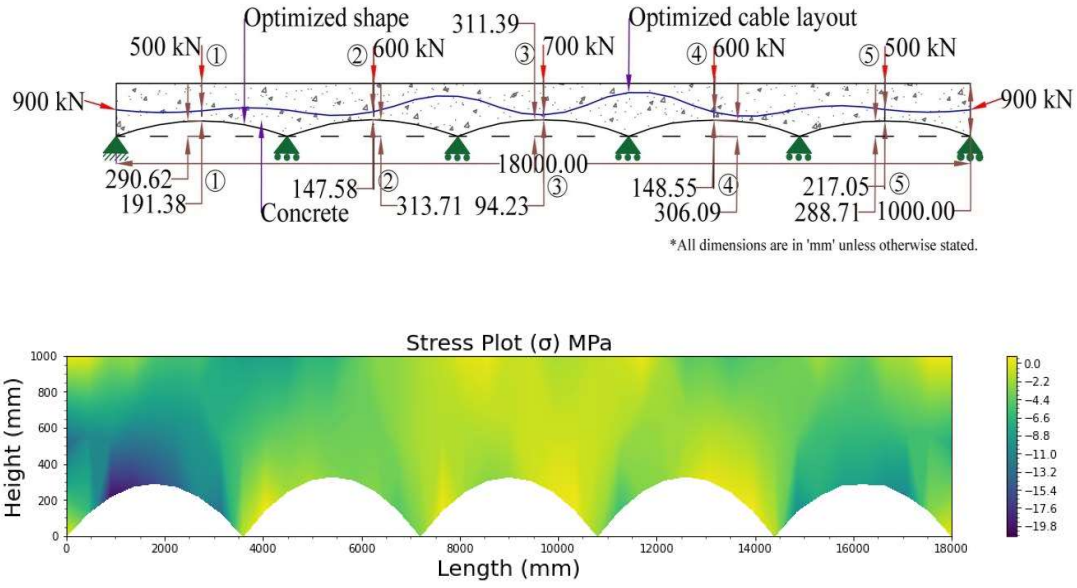
Optimized shape
311.39
Optimized cable layout
500 kN
600 kN
700 kN
600 kN
500 kN
900 kN
900 kN
290.62
191.38
147.58
Concrete
313.71
94.23
18000.00
148.55
306.09
217.05
288.71
1000.00
*All dimensions are in 'mm' unless otherwise stated.
Stress Plot (σ) MPa
Height (mm)
Length (mm)

(c)

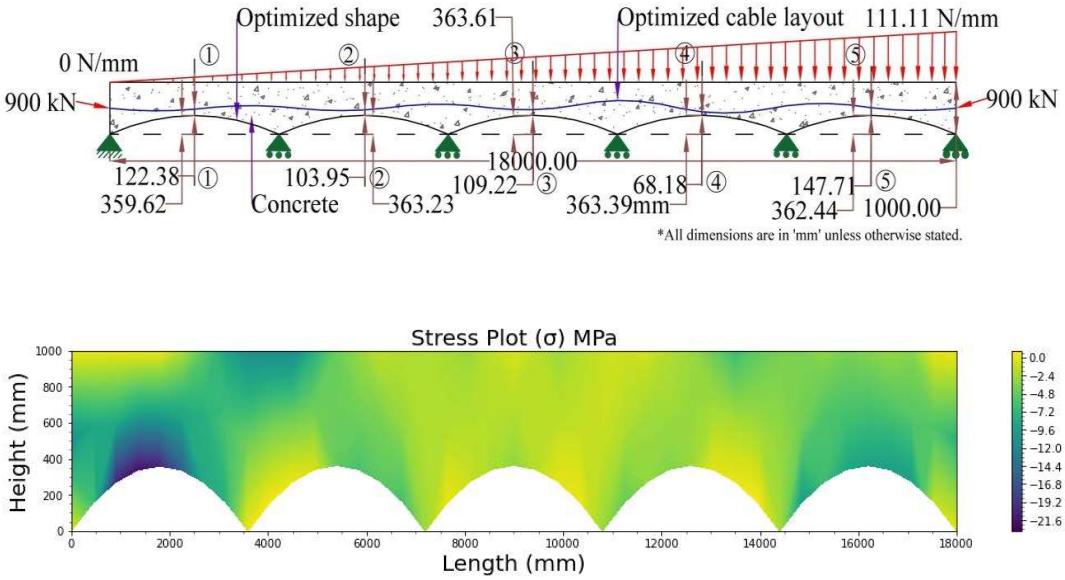

(d)

Figure 6.10: Optimized concrete shape, cable layout and Stress distribution plot of P_{B3} for (a) MPL without frictional loss, (b) UIL without frictional loss, (c) MPL with frictional loss, and (d) UIL with frictional loss

6.10 Discussion

From the models discussed in Section 6.9, it can be deduced that the SSCO is capable of synergistically optimizing the concrete shape and cable layout of PSC beams for any given number of spans, imposed load and pre-stressing force. The optimized shape doesn't induce new cavities in the beam and modifies only the outer boundary. The number of iterations to reach the optimized state varies from 3 to 6, with the total runtime being less than 1 second, as inferred from Table 2-4. The beams P_{B1}, P_{B2}, and P_{B3} in their optimized state are pushed to the compressive zone from their initial tensile zone for all the cases of loading. An overall weight reduction ranging from 12% to 24% is achieved in different models as per the type of PSC beam and imposed loading over it. It is also noted that for beam P_{B1} the δ at Section 1-1 decreases for the optimized state

by almost a factor of 2 with respect to its initial state. However, in beam P_{B2} it is observed that the δ for the optimized state decreases at Section 1-1 and 3-3, whereas it increases for Section 2-2 in comparison to its initial state. Similarly in P_{B3} the δ decreases in Sections 1-1, 3-3, and 5-5 but increases in Sections 2-2 and 4-4. From this, it can be inferred that the δ starts decreasing from the end span and then follows an alternate increasing and decreasing pattern in its optimized state with respect to its initial state.

Further, In beam P_{B3}, it can be observed that in Section 5-5, when we ignore the frictional loss, the distance between the initial and optimized boundary is 296.88mm, with the distance between the cable layout and optimized concrete boundary being 185.12mm as shown in Figure 6.10(a), however, when the frictional loss is considered the distance between initial and optimized boundary is 288.71mm with the distance between cable layout and optimized concrete boundary being 217.05mm as shown in Figure 6.10(c). This variation in co-ordinates of both cable layout and concrete shape stemming due to the ignorance and consideration of friction loss accounts that the SSCO is sensitive to the loss in pre-stressing force along the span of the beam and modifies both the cable layout and concrete shape as per the actual pre-stressing force at that section. Accounting for the final concrete shape, the beam P_{B2} forms an overall concave shape along the full length of the beam in the final optimized state, as shown in Figure 6.8. This is because in beam P_{B2} the movement of intermediate supports is allowed in accordance with the boundary of concrete, whereas in P_{B3}, where the intermediate supports are not allowed to move, it forms a span-wise concave shape in the final optimized state, as shown in Figure 6.10.

6.11 Concluding remark

The present work exhibits a new approach towards achieving a synergistically optimized cable layout and concrete shape for PSC beams. The entire approach is packaged as a software labelled SSCO coded in FORTRAN language. The shape of the concrete is modified from the boundaries without forming any new cavities, and the cable profile is modified accordingly to bring σ_{top} and σ_{bottom} under compression (< 0.5 N/mm^2) at the selected sections. Using the proposed methodology, three different PSC beams having different spans, cross-sections, lengths, imposed loading, and pre-stressing force have been successfully optimized to obtain an optimum concrete shape and cable layout, results of which are presented in Section 6.9. The PSC beams in their optimized state save 12% to 24% of material compared to their initial state without producing any abnormally high deflection. The influences of frictional loss on the overall optimum concrete shape and cable layout have also been successfully demonstrated. It can be observed that the proposed approach offers a holistic tool that can be used by industries to achieve an optimized cable layout and concrete shape for PSC beams that are easy to fabricate.